

# Valence Bond Concepts Applied to the Molecular Mechanics Description of Molecular Shapes. 3. Applications to Transition Metal Alkyls and Hydrides

Clark R. Landis,\* Thomas Cleveland, and Timothy K. Firman

Contribution from the Department of Chemistry, University of Wisconsin—Madison, 1101 University Avenue, Madison, Wisconsin 53706-1396

Received October 6, 1997. Revised Manuscript Received January 9, 1998

**Abstract:** Recently we reported a qualitative, valence bond derived model for describing the shapes of transition metal complexes, with a focus on metal hydrides and alkyls. This model, based on the concepts of hybridization and resonance, rationalizes the unusual and varied shapes of hydride and alkyl complexes with transition metals. This paper demonstrates the quantitative incorporation of these valence bond concepts into molecular mechanics algorithms. The resulting force field method (HV-VB) accurately describes the structures of alkyls and hydride complexes of the transition metals. For a wide variety of crystallographically characterized molecules, the HV-VB computations faithfully reproduce the observed structures.

## Introduction

The development of molecular mechanics (MM) models for describing the shapes of transition metal complexes is complicated. Previous MM approaches to transition metals have relied on (1) identification of an idealized, predetermined shape,<sup>1–3</sup> (2) steric repulsion between ligands,<sup>4–10</sup> or (3) the incorporation of ligand-field perturbations of d-electron energies.<sup>11</sup> We have shown that valence bond concepts, such as hybridization and resonance, may be developed into robust MM algorithms for normal and hypervalent main group compounds.<sup>12,13</sup> Qualitatively, we have demonstrated that the concepts of hybridization and resonance lead to unique insights into the factors controlling the shapes of transition metal alkyl and hydride complexes.<sup>14–17</sup> This paper discusses the application of the Hypervalent-VALBOND (HV-VB) MM method to computing the shapes of transition metal hydride and alkyl complexes.

We have implemented the basic principles of hybridization and resonance into MM force fields<sup>12,13</sup> for the study of transition metal complexes. The primary difference between transition metal and main group applications concerns the

valence orbital set. Main group elements make use of the valence s and p orbitals in forming bonds, whereas transition metals make use of the valence s and d orbitals. Differences in the shapes of the  $sp^n$  versus  $sd^n$  hybrid orbitals give rise to contrasting geometries even when valence electron counts are the same. Because there are more orbitals in the d set than the p set, it is possible to have a higher number of valence electrons allowed in transition metal compounds before considerations of hypervalency and resonance must be made.

In this paper we demonstrate the utility of the HV-VB MM computational method when applied to transition metal alkyl and hydride complexes. The significance of this work is 2-fold. First the HV-VB method is, to the best of our knowledge, the only empirical force field method capable of describing the diversity of structures exhibited by transition metal hydride and alkyl complexes. Second, the computations provided herein constitute strong quantitative support for VB-based descriptions of transition metal molecular shapes. First we describe the methods used in our calculations, then the results of these computations for both nonhypervalent and hypervalent complexes are compared with structures derived from X-ray crystallography determinations, gas-phase electron diffraction experiments, and ab initio quantum mechanical electronic structure computations.

## Computational Methods

The ab initio computations presented here were performed by using the DFT(B3LYP) method in PS-GVB.<sup>18–20</sup> The double- $\xi$  Hay and Wadt basis sets, with an effective core potential of all but the valence and penultimate shell, were used for the transition metals.<sup>21–24</sup> Lighter elements were represented with the 6-31G\*\* basis set.

We will refer to our MM computational method as HV-VB, indicating that we are using algorithms based on the treatment of hypervalent molecules published by Landis and Cleveland.<sup>13</sup> We note that the HV-VB method treats nonhypervalent molecules as well. The

(1) Allured, V. S.; Kelly, C.; Landis, C. R. *J. Am. Chem. Soc.* **1991**, *113*, 1–12.

(2) Rappé, A. K.; Casewit, C. J.; Colwell, K. S.; Goddard, W. A. I.; Skiff, W. M. *J. Am. Chem. Soc.* **1992**, *114*, 10024–10035.

(3) Mayo, S. L.; Olafson, B. D.; Goddard, W. A., III *J. Phys. Chem.* **1990**, *94*, 8897–3924.

(4) Vedani, A. *J. Comput. Chem.* **1988**, *9*, 269–280.

(5) Vedani, A.; Huhta, D. W. *J. Am. Chem. Soc.* **1990**, *112*, 4759–4767.

(6) Hay, B. P. *Inorg. Chem.* **1991**, *30*, 2876–2884.

(7) Hay, B. P. *Coord. Chem. Rev.* **1993**, *126*, 177–236.

(8) Lauher, J. W. *J. Am. Chem. Soc.* **1986**, *108*, 1521–1531.

(9) Sironi, A. *Inorg. Chem.* **1992**, *31*, 2467–2475.

(10) Sironi, A. *J. Chem. Soc., Dalton Trans.* **1993**, 173–178.

(11) Burton, V. J.; Deeth, R. J.; Kemp, C. M.; Gilbert, P. J. *J. Am. Chem. Soc.* **1995**, *117*, 8407–8415.

(12) Root, D. M.; Landis, C. R.; Cleveland, T. *J. Am. Chem. Soc.* **1993**, *115*, 4201–4209.

(13) Cleveland, T.; Landis, C. R. *J. Am. Chem. Soc.* **1996**, *118*, 6020–6030.

(14) Landis, C. R.; Cleveland, T.; Firman, T. K. *J. Am. Chem. Soc.* **1995**, *117*, 1859–1860.

(15) Landis, C. R.; Cleveland, T.; Firman, T. K. *Science* **1996**, *272*, 179.

(16) Landis, C. R. *Adv. Mol. Res.* **1996**, *2*, 129.

(17) Landis, C. R.; Firman, T. K.; Root, D. M.; Cleveland, T. Submitted for publication.

(18) Lee, C.; Yang, W.; Parr, R. G. *Phys. Rev. B* **1988**, *37*, 785–789.

(19) Becke, A. D. *Phys. Rev. A* **1988**, *38*, 3098.

(20) Ringnalda, M. N.; Langlois, J.-M.; Murphy, R. B.; Greeley, B. H.; Cortis, C.; Russo, T. V.; Marten, B.; Donnelly, R. E., Jr.; Pollard, W. T.; Cao, Y.; Muller, R. P.; Mainz, D. T.; Wright, J. R.; Miller, G. H.; Goddard, W. A., III; Friesner, R. A. P5-GVB v2.3, Schrodinger, Inc., 1996.

**Table 1.** Metal-Centered Hybridizations for Some Transition Metal Hydrides

VALBOND		VALBOND	
compd	bond hybridization	compd	bond hybridization
YH <sub>2</sub> <sup>+</sup>	sd <sup>1</sup>	NbH <sub>5</sub>	sd <sup>4</sup>
PdH <sub>2</sub>	sd <sup>1</sup>	TcH <sub>5</sub>	sd <sup>4</sup>
ZrH <sub>3</sub> <sup>+</sup>	sd <sup>2</sup>	MoH <sub>6</sub>	sd <sup>5</sup>
RhH <sub>3</sub>	sd <sup>2</sup>	TcH <sub>6</sub> <sup>+</sup>	sd <sup>5</sup>
RuH <sub>4</sub>	sd <sup>3</sup>	PdH <sub>3</sub> <sup>-</sup>	sd <sup>1</sup> (hypervalent)
ZrH <sub>4</sub>	sd <sup>3</sup>	RhH <sub>4</sub> <sup>-</sup>	sd <sup>2</sup> (hypervalent)
NbH <sub>4</sub> <sup>+</sup>	sd <sup>3</sup>		

HV-VB calculations in this report used a modified version of UFF.<sup>2</sup> Our modifications to UFF2 were the incorporation of the HV-VB algorithms for the angular force field terms. Other differences from UFF2 and the published UFF occur primarily in the description of nonbonded interactions. A full description of the potential energy expression as well as the parameters used can be found in the Supporting Information. All of the computational results presented here neglect any electrostatic contributions to the potential energy function and its derivatives. Nonbonded repulsions were applied to 1,3-interactions as well as to 1,4 and beyond.

For nonhypervalent molecules, the angular potential energy terms are determined from the nonorthogonality of hybrid orbitals. Hybridizations for transition metal to ligand bonds are determined from the following rules:

Rule 1: The s-block and p-block elements form sp<sup>n</sup> hybrids, whereas transition metals form sd<sup>n</sup> hybrids.

Rule 2: For molecules with mixed ligands and/or multiple bonds, the distribution of p and d character among the hybrid orbitals depends on the relative electronegativities of the ligands (Bent's rule) and on the bond orders.

Rule 3: Strong ionic-covalent resonance stabilizes hypervalent centers; such resonance commonly maximizes at a linear arrangement of the electron pair bond and the ligand localized electron pair.

Hybridizations determined by these rules for simple metal complexes are presented in Table 1.

As we have shown previously, given the hybridizations (sp<sup>n</sup>d<sup>m</sup>) for all metal-ligand bonds in a transition metal complex, the potential energy as a function of the bond angle ( $\alpha$ ) may be computed by using expressions 1–6. Equations 1 and 2 define the hybrid orbitals; eq 3 expresses the overlap of the those two hybrid orbitals.  $S^{\max}$  represents the maximum value of the hybrid orbital wave functions, which is obtained at bond angles for which the hybrids are perfectly orthogonal. The term  $S(\alpha)$  is the hybrid orbital strength as a function of the bond angle. We refer to the term  $S^{\max} - S(\alpha)$  as the pair defect, i.e., the loss of hybrid orbital concentration in the bonding region due to hybrid orbital nonorthogonality. The parameter  $k$  is a scaling constant that scales the pair defect to energy units.

$$hy_1 = \sqrt{\frac{1}{1+m+n}}(1s + \sqrt{m}p_z + \sqrt{n}dz^2) \quad (1)$$

$$hy_2 = \sqrt{\frac{1}{1+m+n}} \left( 1s + \sqrt{m} \left[ \cos \alpha p_z + \sin \alpha p_x + \sqrt{n} \left( \frac{1}{2} \times (3 \cos^2 \alpha - 1) dz^2 + \frac{\sqrt{3}}{2} \sin^2 \alpha dx^2 - y^2 + \sqrt{3} \sin \alpha \cos \alpha dz \right) \right] \right) \quad (2)$$

$$\Delta = \frac{1}{1+m+n} \left( 1 + m \cos \alpha + \frac{n}{2} (3 \cos^2 \alpha - 1) \right) \quad (3)$$

$$S^{\max} = \sqrt{\frac{1}{1+m+n}} (1 + \sqrt{3m} + \sqrt{5n}) \quad (4)$$

$$S(\alpha) = S^{\max} \sqrt{1 - \frac{1 - \sqrt{(1 - \Delta^2)}}{2}} \quad (5)$$

$$E = k(S^{\max} - S(\alpha)) \quad (6)$$

During the course of working on these and other computations it was determined that a modification of the previously reported HV-VB algorithms would not only give better results, but also yield a model that was more closely aligned with the valence bond concepts on which it was developed.

The previously published HV-VB method treated hypervalent molecules by creating an ensemble of molecular mechanics resonance configurations—one resonance configuration per 3 center-4 electron bond. The MM configurations were weighted by a geometry dependent weighting factor ( $c_i$ ) that is based on the angles formed by the ligands involved in 3 center-4 electron bonds (eq 7).

$$c_i = \frac{\prod_{i=1}^{\text{hype}} \cos^2 \theta_i}{\sum_{j=1}^{\text{res}} \prod_{i=1}^{\text{hype}} \cos^2 \theta_i} \quad (7)$$

The resonance configuration weighting function shown in eq 7 favors resonance configuration with linear 3 center-4 electron bonds and disfavors bent arrangements. This scheme works well for hypervalent main group compounds, primarily because these molecules have predominately p-character in their bonds.<sup>13</sup> Effectively, resonance stabilization of a 3 center-4 electron bond maximizes with increasing overlap of the two bond-forming hybrid orbitals; for molecules with sp<sup>n</sup> hybridization this overlap is modeled well with a cos<sup>2</sup> function. The shapes of transition metal hybrid orbitals with more than 67% d-character (e.g., sd<sup>3</sup>) are more complex, having two nodal cones.

To better model the angular dependence of 3 center-4 electron resonance interactions involving sd<sup>n</sup> hybrids, we have adopted an overlap-dependent weighting function (eqs 8 and 9). According to this function, placements of ligands in the nodal cones are the worst possible arrangement for stabilization due to 3 center-4 electron bonding (Figure 1). It should also be noted that the use of this new function does not introduce any additional parameters. The hybridizations used in the weighting function are identical to those used by the standard HV-VB potential energy term.

$$c_i = \frac{\prod_{i=1}^{\text{hype}} \Delta_i^2}{\sum_{j=1}^{\text{res}} \prod_{i=1}^{\text{hype}} \Delta_i^2} \quad (8)$$

$$\Delta = \frac{1}{1+m+n} \left( 1 + m \cos \alpha + \frac{n}{2} (3 \cos^2 \alpha - 1) \right) \quad (9)$$

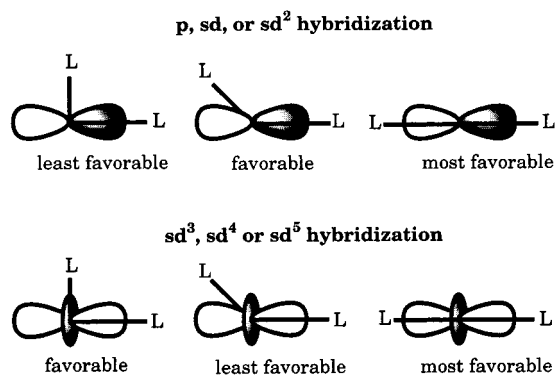
The only fitted parameters for the HV-VALBOND computations of transition metal complexes are the scaling constants ( $k$  in eq 6). These parameters, for which we have used just one value per transition metal, have values that were set by comparison of VALBOND vibrational frequencies to DFT frequencies for a small set of transition metal hydrides (see Table 2). Parameters for the remaining transition metals were determined by interpolation/extrapolation from these values. Our focus is the computation of molecular shapes. We stress metal covalent radii were not adjusted to achieve better fits between computed and crystallographic metal-ligand distances in this work. All geometry optimizations of structures for comparison with crystallographic results were started from the crystallographic coordinates. Newton-Raphson minimization to a gradient root mean square of at most  $1.0 \times 10^{-5}$  was performed.

(21) Hay, P. J.; Wadt, W. R. *J. Chem. Phys.* **1985**, *82*, 271–284.

(22) Hay, P. J.; Wadt, W. R. *J. Chem. Phys.* **1985**, *82*, 285–298.

(23) Hay, P. J.; Wadt, W. R. *J. Chem. Phys.* **1985**, *82*, 299–310.

(24) Breidung, J.; Thiel, W.; Komornicki, A. *Chem. Phys. Lett.* **1988**, *153*, 76–81.



**Figure 1.** Schematic representation of orbital shapes with different orientations of ligands involved in 3 center-4 electron bonds.

**Table 2.** DFT(B3LYP) and VALBOND Vibrational Frequencies (cm<sup>-1</sup>) for Select Metal Hydrides

	DFT	VALBOND		DFT	VALBOND
PdH <sub>2</sub>	637	638	NiH <sub>2</sub>	676	683
rms 42.8	2039	2066	rms 7.6	2042	2047
	2150	2081		2058	2068
PtH <sub>2</sub>	815	812	FeH <sub>4</sub>	823	710
rms 14.7	2333	2341	rms 86.8	823	710
	2379	2355		823	710
				828	949
RuH <sub>4</sub>	762	726		828	949
rms 42.1	762	726		1980	1982
	762	726		1980	1982
	925	985		1980	1982
	925	985		1993	1979
	1860	1873			
	1860	1873	MoH <sub>6</sub>	694	701
	1860	1873	rms 23.3	694	728
	1939	1873		754	742
				787	790
OsH <sub>4</sub>	775	701		959	804
rms 78.5	775	701		959	899
	775	701		1014	901
	826	957		1014	952
	826	957		1070	1318
	2183	2203		1845	1816
	2183	2203		1845	1824
	2183	2203		1910	1838
	2264	2205		1946	1924
				1952	1958
				1952	2042

The electron diffraction patterns of Ta(Me)<sub>5</sub> and W(Me)<sub>6</sub> have been simulated by using molecular dynamics with the UFF/VALBOND algorithms. Both dynamics runs were at 294 K, simulating a period of 1.9 ns with dynamics steps every 10 fs. A total of 1892 updates (one per ps), or "snapshots", of the molecule were saved. Only steps 200–1892 were used; the first 199 steps were omitted to allow the dynamics simulation to equilibrate the temperature. Cerius2 2.0<sup>25</sup> was used to display the results and to determine when the simulated temperature equilibrated. Several pairs of carbons were examined in both compounds and were found to occasionally alternate between having acute angles and obtuse ones, demonstrating that the methyl groups were interchanging at this time scale, which we would expect given the low barriers associated with interconversion in both cases.

$$I_{\text{Simulated}}(s) = \sum_{i,j} \left[ \frac{f_i(s) \cdot f_j(s) \cos[\eta_i(s) - \eta_j(s)]}{1693} \sum_{k=200}^{1892} \left( \frac{\sin(s \cdot r_{ij}(k))}{s \cdot r_{ij}(k)} \right) \right] \quad (10)$$

$s \equiv (4\pi/\lambda)\sin(\theta)$  and  $r_{ij}(k) \equiv$  distance between atoms  $i$  and  $j$  in update number  $k$ .

(25) Molecular Simulations, Inc.: San Diego, CA.

Molecular scattering intensities were simulated according to eq 10. Values for  $f(s)$  and  $\eta(s)$  were obtained from the International Tables,<sup>26</sup> or were interpolated from them.  $I(s)$  was evaluated at the same  $s$  values that it was measured at in the experiment. In addition,  $I(s)$  was evaluated at values  $s < 2$ , which are impractical to determine experimentally, and so were simulated in the original experiment. The simulated values were modified according to eq 11, as the experimental ones were, and  $I_{\text{mod}}$  was Fourier transformed to generate the radial distribution plot.

$$I_{\text{Mod}}(s) = \frac{s}{f_M f_C} e^{-0.004s^2} \cdot I_{\text{Simulated}}(s) \quad (11)$$

**Results for Nonhypervalent Complexes.** Ab initio DFT(B3LYP) calculations, as well as crystal structures, were used to test the accuracy of the VALBOND method. A comparison of structures predicted by DFT and VALBOND can be seen in Table 3. The general features of the potential energy surfaces are modeled well by the VALBOND force field, with some of the finer details in disagreement between the two methods. An almost one-to-one correspondence in the shapes of the minima is found between the two methods. In the cases with multiple minima, however, the ordering of the minima do not agree.

The compounds with sd and sd<sup>2</sup> hybridized bonds prefer 90° bond angles according to the VALBOND potential energy function. Deviations between VALBOND and DFT structures are small with larger errors for the sd<sup>2</sup> hybridized compounds. Larger differences for sd<sup>2</sup> hybridization can be understood by focusing on the minima in the potential energy functions that are used for these two hybridizations (Figure 2). The sd<sup>2</sup> minimum is broader and shallower, hence molecules are floppier.

RuH<sub>4</sub> is sd<sup>3</sup> hybridized and yields three minima on the HV-VB surface, with the tetrahedral geometry having the lowest energy conformation. DFT computations also find a tetrahedral minimum, but the C<sub>4v</sub> geometry is the lowest energy conformation on the DFT potential energy surface. Interestingly, the DFT surface does not have a minimum at the C<sub>3v</sub> geometry. Why should RuH<sub>4</sub> exhibit such a complex geometry? Qualitatively, we have shown that all three idealized structures with sd<sup>3</sup> bond hybridization are generated by placing H's on the vertexes of a cube such that no two H's are trans. HV-VB computations on RuH<sub>4</sub> yield a complex potential energy surface with three local minima because of the dual-welled nature of the sd<sup>3</sup> hybrid orbital strength function.

The sd<sup>4</sup> hybridized WH<sub>5</sub><sup>+</sup> compound has six minima on the HV-VB potential energy surface. Two C<sub>4v</sub> structures and a C<sub>3v</sub> form the highest symmetry minima; the global minimum is the square-pyramidal, C<sub>4v</sub> structure. Both C<sub>4v</sub> structures are found by DFT computations also; however, the umbrella C<sub>4v</sub> structure is the global minimum. DFT computations support the predictions of the HV-VB method: only one of the six minima found by the HV-VB method is not a minimum on the DFT surface. Both DFT and HV-VB computations yield structures having bond angles clustered around 70° and 118°, close to the idealized sd<sup>4</sup> bond angles of 66° and 114°. The complexity of the WH<sub>5</sub><sup>+</sup> surface is rationalized readily. There is no single geometry in which all five ligands make only the idealized 66° and 114° bond angles preferred by sd<sup>4</sup> hybridization. From this viewpoint, WH<sub>5</sub><sup>+</sup> is intrinsically strained and can adopt many structures which are approximately equal in minimizing this strain. Thus, HV-VB not only provides a rapid computational method for modeling these interesting hydride but also provides strong quantitative support for the valence bond model upon which the computations are based.

Previously we have published<sup>14</sup> the HV-VB results for the archetypical sd<sup>5</sup> hybridized compound, WH<sub>6</sub>, the results of which are essentially identical to high level ab initio computations.<sup>27,28</sup>

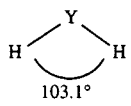
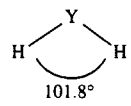
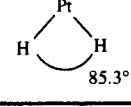
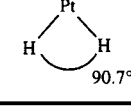
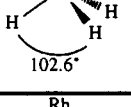
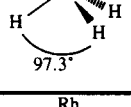
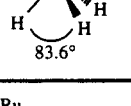
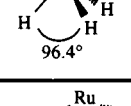
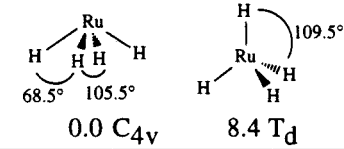
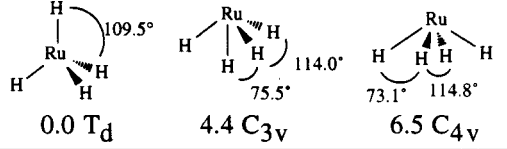
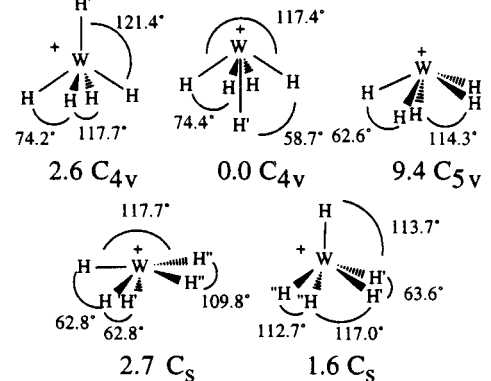
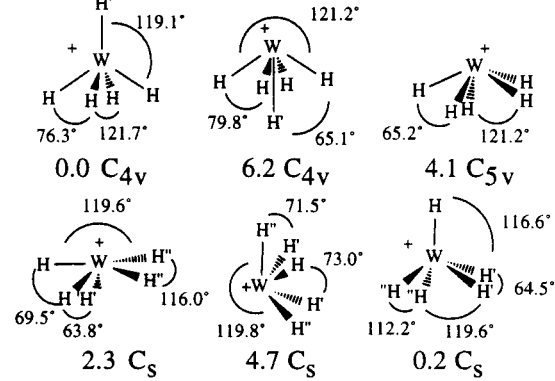
Most experimentally determined nonhypervalent, transition metal alkyl structures have sd<sup>3</sup> hybridization according to our hybridization rules. We found no examples of nonhypervalent sd hybridized alkyl

(26) *International Tables for Crystallography*; Wilson, A. J. C., Ed.; Kluwer Academic Publishers: Dordrecht, The Netherlands, 1995; Vol. C.

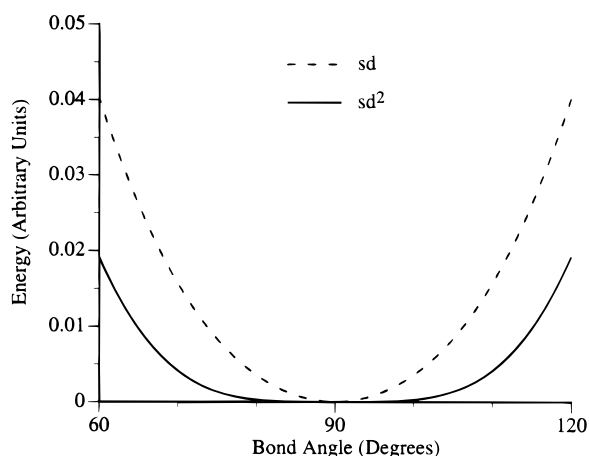
(27) Kang, S. K.; Tang, H.; Albright, T. A. *J. Am. Chem. Soc.* **1993**, *115*, 1971–1981.

(28) Tanpipat, N.; Baker, J. J. *Phys. Chem.* **1996**, *100*, 19818–19823.

**Table 3.** Comparison of DFT(B3LYP) to VALBOND Structures for Nonhypervalent Hydride Complexes<sup>a</sup>

	DFT	VALBOND
$\text{YH}_2^+$ sd	 103.1° $C_{2v}$	 101.8° $C_{2v}$
$\text{PtH}_2$ sd	 85.3° $C_{2v}$	 90.7° $C_{2v}$
$\text{ZrH}_3^+$ sd <sup>2</sup>	 102.6° $C_{3v}$	 97.3° $C_{3v}$
$\text{RhH}_3$ sd <sup>2</sup>	 83.6° $C_{3v}$	 96.4° $C_{3v}$
$\text{RuH}_4$ sd <sup>3</sup>	 0.0 $C_{4v}$ 8.4 $T_d$	 0.0 $T_d$ 4.4 $C_{3v}$ 6.5 $C_{4v}$
$\text{WH}_5^+$ sd <sup>4</sup>	 2.6 $C_{4v}$ 0.0 $C_{4v}$ 9.4 $C_{5v}$ 2.7 $C_s$ 1.6 $C_s$	 0.0 $C_{4v}$ 6.2 $C_{4v}$ 4.1 $C_{5v}$ 2.3 $C_s$ 4.7 $C_s$ 0.2 $C_s$

<sup>a</sup> Relative energies (kcal/mol) are given for compounds exhibiting multiple minima. Bond hybridizations are given for each complex.

**Figure 2.** Comparison of sd and sd<sup>2</sup> potential energy functions.

complexes, and only a few with sd<sup>2</sup> hybridization. The comparison between crystal structure and VALBOND results can be seen in Table 4.

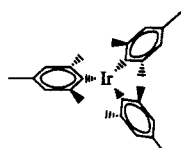
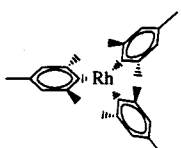
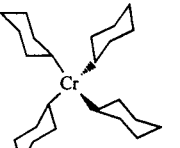
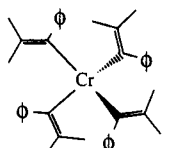
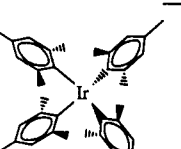
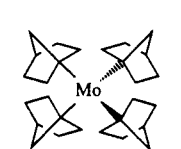
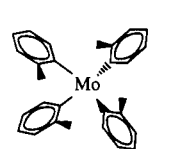
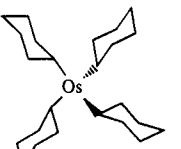
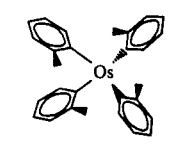
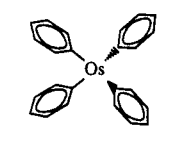
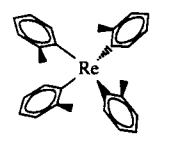

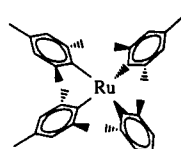
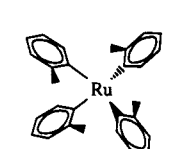
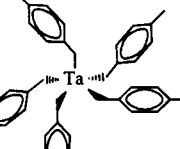
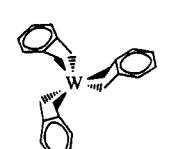
The two sd<sup>2</sup> complexes, Ir(mesityl)<sub>3</sub> and Rh(mesityl)<sub>3</sub>, are pyramidal both by HV-VB computations and X-ray crystallography. This is expected, as the potential energy function for the sd<sup>2</sup> hybrid has one minimum at 90°. In both DFT and VALBOND cases the structures have larger bond angles than the preferred 90° bond angle, due to steric

effects, though they are still considerably smaller than 120° trigonal planar angles. Although formally Ir(III) and Rh(III) complexes often exhibit structures based on an octahedral framework, the valence bond model clearly distinguishes between the T-shape (or meridionally trivalent octahedron) and the trigonal pyramid (or facially trivalent octahedron), with the latter strongly preferred despite its increased steric congestion.

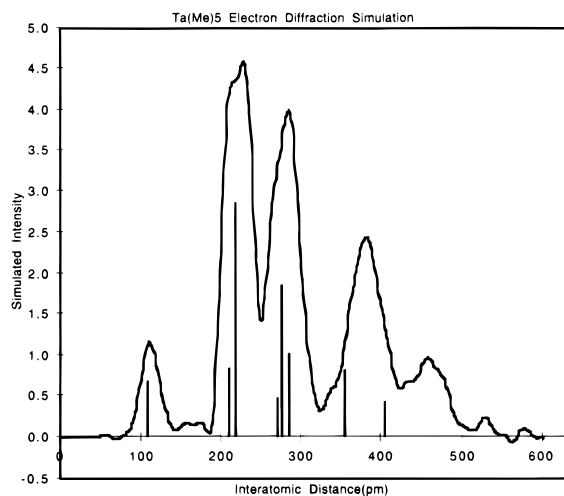
There are numerous examples of sd<sup>3</sup> hybridized transition metal complex crystal structures. The potential energy function for sd<sup>3</sup> hybrids has minima at 71° and 109°. All of the alkyl ligands of these compounds are large enough that their normal van der Waals interactions make the tetrahedron more stable than alternate C<sub>3v</sub> and C<sub>4v</sub> idealized structures. The tetrahedron is the structure on which all of the molecules in this category are based with varying (but always less than ~7°) amounts of distortion. Satisfyingly, structures that show more distortion from tetrahedral in the crystal are those for which the HV-VB method also shows a larger distortion from the base tetrahedron. For the twelve structures examined, the average root-mean-square deviation between MM and crystallographic L–M–L bond angles is just 1.9°.

Ta(*p*-methylbenzyl)<sub>5</sub> has sd<sup>4</sup> hybridized Ta–C bonds. The HV-VB calculated structure matches the geometry of the crystal very well; the root-mean-square deviation between the angles of the two complexes is 3.83°. Overall the structure is a distorted square-pyramid. The electron diffraction data for Ta(CH<sub>3</sub>)<sub>5</sub> indicate a square-pyramidal

**Table 4.** Results for Nonhypervalent Transition Metal Complexes Comparing Crystal Structures to VALBOND Calculated Results<sup>k</sup>

 JURLUD VALBOND XTAL <sup>a</sup> Ir-C 1.916 2.001 sd <sup>2</sup> 110.5 106.1 113.7 106.5 RMS 114.0 109.9 5.42	 VEZNDX VALBOND XTAL <sup>b</sup> Rh-C 1.992 1.967 sd <sup>2</sup> 103.7 103.8 107.9 104.5 RMS 108.0 105.7 2.37	 FEFTUF VALBOND XTAL <sup>c</sup> Cr-C 2.075 2.010 sd <sup>3</sup> 106.3 106.2 106.3 106.2 RMS 106.4 107.8 1.10 106.4 107.8 115.8 114.5 115.8 114.5	 MPEYCR VALBOND XTAL <sup>d</sup> Cr-C 2.116 2.034 sd <sup>3</sup> 107.4 105.1 107.7 105.3 RMS 107.1 107.0 2.03 107.4 107.4 113.3 116.2 114.0 116.3
 JURMEO VALBOND XTAL <sup>a</sup> Ir-C 1.961 2.017 sd <sup>3</sup> 100.1 95.4 100.1 96.4 RMS 114.3 114.8 3.18 114.3 117.8 114.4 116.8 114.4 117.0	 GIMKUI VALBOND XTAL <sup>e</sup> Mo-C 1.989 2.085 sd <sup>3</sup> 108.6 109.1 108.7 109.1 RMS 109.6 109.5 0.42 109.6 109.5 109.4 109.5 110.9 110.1	 KAYJID VALBOND XTAL <sup>f</sup> Mo-C 2.005 2.085 sd <sup>3</sup> 101.9 108.5 107.7 108.5 RMS 108.5 108.5 3.61 108.7 108.5 112.0 111.5 117.3 111.5	 DAJLUV VALBOND XTAL <sup>c</sup> Os-C 1.993 2.029 sd <sup>3</sup> 107.2 105.4 107.2 105.4 RMS 107.2 106.3 2.09 107.2 106.3 114.0 117.1 114.2 117.1
 DAJMAG VALBOND XTAL <sup>g</sup> Os-C 2.000 1.997 sd <sup>3</sup> 107.1 106.1 107.1 106.1 RMS 107.7 106.9 0.81 107.7 106.9 113.6 114.1 117.6 117.0	 FEFTOZ VALBOND XTAL <sup>c</sup> Os-C 1.987 1.995 sd <sup>3</sup> 108.6 107.6 108.6 107.6 RMS 109.9 110.4 0.71 109.9 110.4 109.9 110.4 109.9 110.4	 FURTAN VALBOND XTAL <sup>h</sup> Re-C 2.026 2.030 sd <sup>3</sup> 103.3 105.6 104.6 107.4 RMS 112.8 108.8 2.60 112.4 109.3 111.7 112.4 112.3 113.4	 FEFVAN VALBOND XTAL <sup>c</sup> Ru-C 1.847 2.019 sd <sup>3</sup> 107.0 105.4 107.0 105.4 RMS 107.0 107.6 1.39 107.1 107.6 114.4 116.0 114.5 116.3
 JURMAK VALBOND XTAL <sup>a</sup> Ru-C 1.890 2.011 sd <sup>3</sup> 98.8 99.1 98.8 99.6 RMS 115.1 112.5 1.57 115.1 113.6 115.0 116.0 115.0 117.0	 FURTER VALBOND XTAL <sup>h</sup> Ru-C 1.846 1.995 sd <sup>3</sup> 101.8 106.3 110.6 106.3 RMS 108.6 107.8 3.29 109.3 107.8 109.4 113.9 116.7 114.9	 HEDKUW VALBOND XTAL <sup>i</sup> Ta-C 2.129 2.194 sd <sup>4</sup> 80.5 80.6 80.5 81.9 RMS 82.7 82.8 3.83 86.5 84.6 109.5 104.7 110.9 107.5 105.8 113.7 118.3 118.2 132.0 137.0 142.5 138.1	 OXYLDW VALBOND XTAL <sup>j</sup> W-C 2.070 2.208 sd <sup>5</sup> 73.0 74.7 73.0 74.7 RMS 73.0 74.7 1.33 87.6 86.6 87.6 86.6 87.6 86.6 89.5 87.4 89.5 87.4 89.5 87.4 89.5 87.4 132.4 132.6 132.4 132.6 132.4 132.6 133.0 133.7 133.0 133.7

<sup>a</sup> Hay-Motherwell, R. S.; Wilkinson, G.; Hussain-Bates, B.; Hursthouse, M. B. *J. Chem. Soc., Dalton Trans.* **1992**, 3477. <sup>b</sup> Hay-Motherwell, R. S.; Hussain-Bates, B.; Hursthouse, M. B.; Wilkinson, G. *J. Chem. Soc., Chem. Commun.* **1990**, 1242. <sup>c</sup> Stavropoulos, P.; Savage, P. D.; Toozee, R. P.; Wilkinson, G.; Hussain, B.; Motevalli, M.; Hursthouse, M. B. *J. Chem. Soc., Dalton Trans.* **1987**, 557. <sup>d</sup> Cardin, D. J.; Roy, A. *J. Chem. Soc., Chem. Commun.* **1978**, 899. <sup>e</sup> Kolodziej, R. M.; Schrock, R. R.; Davis, W. M. *Inorg. Chem.* **1988**, *27*, 3253. <sup>f</sup> Arnold, J.; Wilkinson, G.; Hussain, B.; Hursthouse, M. B. *J. Chem. Soc., Dalton Trans.* **1989**, 2149. <sup>g</sup> Toozee, R. P.; Stavropoulos, P.; Motevalli, M.; Hursthouse, M. B.; Wilkinson, G. *J. Chem. Soc., Chem. Commun.* **1985**, 1139. <sup>h</sup> Savage, P. D.; Wilkinson, G.; Motevalli, M.; Hursthouse, M. B. *J. Chem. Soc., Dalton Trans.* **1988**, 669. <sup>i</sup> Piersol, C. J.; Profflet, R. D.; Fanwick, P. E.; Rothwell, I. P. *Polyhedron* **1993**, *12*, 1779. <sup>j</sup> Lappert, M. F.; Raston, C. L.; Skelton, B. W.; White, A. H. *J. Chem. Soc., Chem. Commun.* **1981**, 485. <sup>k</sup> Distances given are averages of all metal-carbon distances. Angles listed in the table are those involving the metal as the central atom. rms deviations are between these lists. The six letter Cambridge Crystallographic Database<sup>29</sup> codes are also given. Bond hybridizations are given for each complex.



**Figure 3.** Simulated Ta(CH<sub>3</sub>)<sub>5</sub> electron diffraction radial distribution, with major peaks from the experimental data marked as solid bars.

structure with 111.7° C<sub>apical</sub>-Ta-C<sub>basal</sub> bond angles and 82.2° and 136.8° for the C<sub>basal</sub>-Ta-C<sub>basal</sub> angles. Our HV-VB computations yield values of 116.7° (C<sub>apical</sub>-Ta-C<sub>basal</sub>) and 78.3° and 126.5° (C<sub>basal</sub>-Ta-C<sub>basal</sub>). Although five-coordinate complexes are often considered to have low energy distortions to nearly isoenergetic trigonal bipyramidal structures, the valence bond model suggests that nonhypervalent molecules with sd<sup>4</sup> hybridization will strongly prefer the distorted square pyramid, as borne out by experiment.

We previously have reported the structure calculated by our method of one sd<sup>5</sup> hybridized complex, W(Me)<sub>6</sub>.<sup>15</sup> The distorted trigonal prismatic geometry that was predicted for this complex is virtually identical to that found by Pfenning and Seppelt in the crystal structure. HV-VB accurately reproduces the structure of another sd<sup>5</sup> tungsten complex W(*o*-xylylene)<sub>3</sub>, giving rise to a root-mean-square deviation between the crystal and HV-VB angles about the central atom of 1.3°.

**Modeling Gas-Phase Electron Diffraction Data.** Perhaps the greatest advantage of force field methods over other methods is the speed of computation, which we have utilized in simulating the gas-phase electron diffraction data for Ta(CH<sub>3</sub>)<sub>5</sub><sup>30</sup> and W(CH<sub>3</sub>)<sub>6</sub>.<sup>31</sup> at room temperature. Because electron diffraction experiments are subject to conformational ensemble averaging, we reasoned that our ability to simulate electron diffraction data was a good test of the overall quality of our molecular mechanics potential energy surfaces. The resulting spectra are shown in Figures 3 and 4.

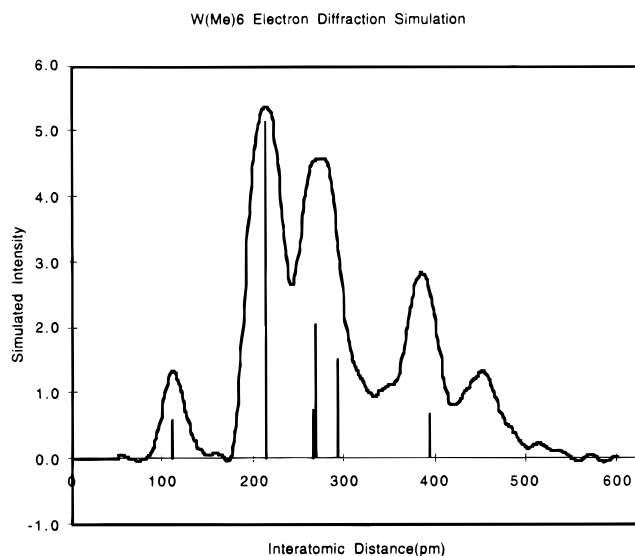
For Ta(CH<sub>3</sub>)<sub>5</sub>, all of the peaks below 300 pm are quite close to the experimental peaks, including the asymmetric shoulder on the peak near 215 pm. However, the two broad peaks representing different C-C distances in the experiment at 355(3) and 405(4) pm are collapsed into one peak at 383 pm in our simulation. At its 0 K geometry, the HV-VB structure of Ta(CH<sub>3</sub>)<sub>5</sub> has nearly equal C<sub>axial</sub>-Ta-C<sub>basal</sub> and trans C<sub>basal</sub>-Ta-C<sub>basal</sub> bond angles, forcing these C-C peaks together in the radial distribution plot. The peaks greater than 400 pm, which were unassigned in the experiment, are H-H distances. One other difference between simulation and experiment is that the peaks at large distances are significantly larger than in the experiment. This arises from differences in the small angle *I*(*s*) values, which are modeled in the experimental spectrum but are computed exactly in the simulation.

The simulated W(CH<sub>3</sub>)<sub>6</sub> electron diffraction radial distribution is shown in Figure 4. The simulation matches the experimental spectrum very well. The only significant difference here is in the farthest C-C peak at around 370 pm, which is a bit too short. Again, the intensities at large distances are greater than those in the experimental spectrum.

(29) Allen, F. H.; Davies, J. E.; Galloy, J. J.; Johnson, O.; Kennard, O.; Macrae, C. F.; Mitchell, E. M.; Mitchell, G. F.; Smith, J. M.; Watson, D. G. *J. Chem. Inf. Comput. Sci.* **1991**, *31*, 187-204.

(30) Pulham, C.; Haaland, A.; Hammel, A.; Rypdal, K.; Verne, H. P.; Volden, H. V. *Angew. Chem., Int. Ed. Engl.* **1992**, *31*, 1464-1467.

(31) Haaland, A.; Hammel, A.; Rypdal, K.; Volden, H. V. *J. Am. Chem. Soc.* **1990**, *112*, 4547-4549.



**Figure 4.** Simulated W(CH<sub>3</sub>)<sub>6</sub> electron diffraction radial distribution, with major peaks from the experimental data marked as solid bars.

In general we find good overall agreement between simulated and experimental gas phase electron diffraction data. The significance of this result is that gas phase electron diffraction is one of the few sources of empirical data that simultaneously contains detailed structural information, is sensitive to conformational averaging, and is free of intermolecular effects. As a result, simulation of electron diffraction data may be employed as a valuable test of force field potential energy surfaces. Conversely, it is possible that molecular dynamics simulations will prove valuable in the analysis of electron diffraction data for complex molecules, much as force field methods have proven invaluable in modeling NMR-derived distances.

**Results for Hypervalent Complexes.** According to our valence bond electron-counting formalism, transition metal centers with more than 12 e<sup>-</sup> are hypervalent. Three cases of hypervalent transition metal hydrides were examined with HV-VB and compared to DFT calculations. The results are summarized in Table 5. The first case is PdH<sub>3</sub><sup>-</sup>, which is sd hybridized with an electron count of 14 e<sup>-</sup>. From a valence bond perspective, this molecule is described as a resonance of among three PdH<sub>2</sub> + H<sup>-</sup> configurations, giving rise to one 3 center-4 electron interaction. PdH<sub>3</sub><sup>-</sup> is structurally and electronically analogous to the main group compound ClF<sub>3</sub>: both compounds have hybridizations that prefer 90° bond angles and one delocalized bonding unit. The DFT structure of PdH<sub>3</sub><sup>-</sup> is very similar to the experimental structure ClF<sub>3</sub>, both showing a slightly arrowhead shape. The HV-VB calculated structures for PdH<sub>3</sub><sup>-</sup> and ClF<sub>3</sub> are very similar, also, both being slightly distorted in the other direction from T-shape.

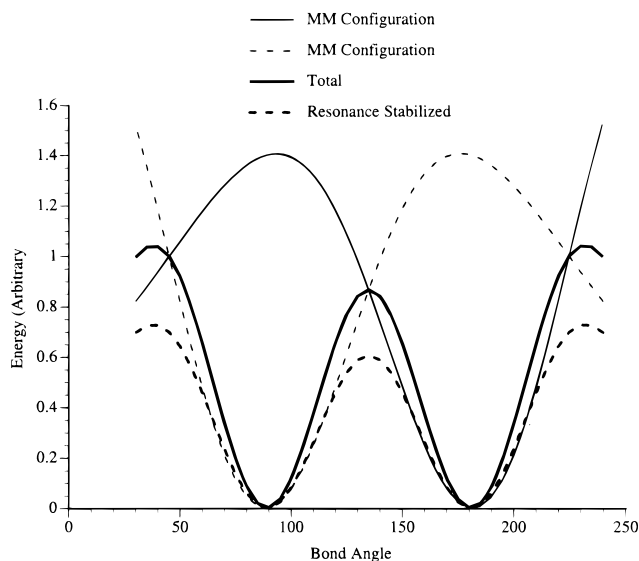
The next example, RhH<sub>4</sub><sup>-</sup>, is the transition metal analogue to SF<sub>4</sub>. Both have hybridizations that prefer 90° bond angles, four ligands and one 3 center-4 electron bond. Again the structural similarities are striking. They are both C<sub>2v</sub>, seesaw geometries with the DFT result for RhH<sub>4</sub><sup>-</sup> and the experimental structure for SF<sub>4</sub> showing the axial ligands bending toward the other pseudoequatorial ligands. As in the previous case, the HV-VB result shows the distortion in the other direction.

WH<sub>7</sub><sup>-</sup>, on the other hand, does not have a simple main group analogue and gives rise to more complicated potential energy surfaces. DFT computations yield two minima separated by 2.96 kcal/mol, and both have C<sub>3v</sub> structures. There are four structures generated by HV-VB within 5 kcal/mol of each other. The HV-VB structures can be generated by looking at the structures for the normal-valent WH<sub>6</sub> and adding a ligand trans to different hydrides. There are only four unique structures that can be generated in this fashion. If the coordinates from the DFT minima are used for the HV-VB computation, energies 4.43 and 9.353 kcal/mol higher than the lowest molecular mechanics structure are obtained for the C<sub>3v</sub> eclipsed and C<sub>3v</sub> staggered, respectively. It should also be noted that these structures are not at minima on the potential energy surface and likewise the molecular mechanics structures are not minima on the ab initio surface.

**Table 5.** Comparison of HV-VB and DFT(B3LYP) Calculated Structures for Hypervalent Hydrides<sup>a</sup>

	DFT	HV-VB
PdH <sub>3</sub> <sup>-</sup> C <sub>2v</sub> sd		
RhH <sub>4</sub> <sup>-</sup> C <sub>2v</sub> sd <sup>2</sup>		
WH <sub>7</sub> <sup>-</sup> sd <sup>5</sup>		

<sup>a</sup> Bond hybridizations are given for each complex.

**Figure 5.** Contribution of resonance structures to the total energy.

One possible source for the discrepancy between the DFT and the HV-VB methods, in the case of WH<sub>7</sub><sup>-</sup>, arises from the lack of explicit resonance stabilization energy. Although the weighting function (eq 8) simulates the correct proportions of MM configurations there is no energetic advantage (resonance energy) to inclusion of additional resonance structures. In Figure 5 the energies of two different configurations are given along with the total energy, as given by the present HV-VB method. When the energies of the two configurations become equal, equal amounts of each MM configuration are added and the total energy comes out to be equivalent to both of the individual MM configurations. Ideally there would be some resonance stabilization when multiple resonance structures are included. A qualitative

resonance-stabilized surface is also shown in Figure 5. The DFT-computed C<sub>3v</sub> minima are structures that involve population of several resonance structures with use of eq 8. The problem with implementation of such a method comes in finding a suitable, generalized algorithm for computing resonance stabilization.

The results for the hypervalent alkyl complexes are summarized in Table 6. One example of a hypervalent sd<sup>0</sup> complex is Mn(C(TMS)<sub>3</sub>)<sub>2</sub>. Despite only having an electron count of 9 e<sup>-</sup>, the complex has one hypervalent interaction due to its high spin (5/2) nature. From our electron-counting rules, the five unpaired electrons occupy pure d orbitals, leaving an s orbital to make one 3 center-4 electron bond. Predominately s bonding gives little orbital directionality; the linear geometry arises from adverse steric effects from the bulky ligands.

All of the sd<sup>1</sup> complexes in Table 6 have two interactions that impact the geometry. The preferences of 90° bond angles between sd<sup>1</sup> hybrid orbitals and linear arrangements of hypervalent interactions lead to a strong preference for these complexes to be square planar. All of the HV-VB structures display a square-planar geometry with small, varying degrees of distortion. For example, the crystal structure of [FePh<sub>4</sub>]<sup>4-</sup> shows a large amount of rectangular distortion (cis bond angles of 119° and 61°). Lithium cations lie above and below the plane between the wide cis angles, suggesting that the rectangular distortion may result from Li-C or Li-Fe interactions.

Compounds with sd<sup>2</sup> hybridization exhibit the widest range of hypervalency, ranging from one to three 3 center-4 electron interactions. As with sd hybrids, sd<sup>2</sup> hybrids prefer 90° bond angles. The resulting structures are based on the octahedron: seesaw (cis divalent octahedron), square pyramidal (monovacant octahedron), and octahedral structures are represented. Two molecules have sd<sup>2</sup> hybridization and deviate considerably from the crystal structures. In the crystal structure of Pt(C<sub>6</sub>Cl<sub>5</sub>)<sub>4</sub> it can be seen that two of the aromatic rings turn so that the *ortho* chlorines are close to the metal. The chlorine-platinum partial bonding interaction was not included in the set of resonance structures modeled by HV-VB, leading to different shapes. The

**Table 6.** Summary of Results for Hypervalent Transition Metal Alkyls<sup>s</sup>

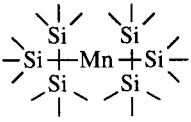
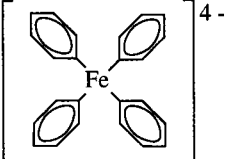
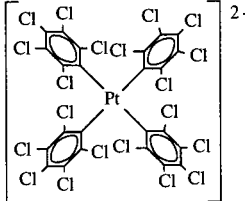
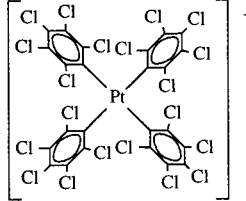
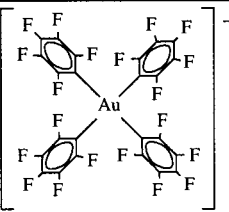
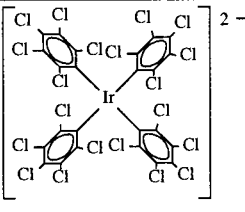
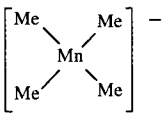
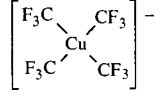
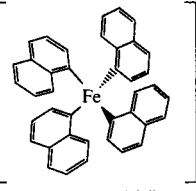
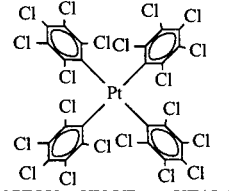
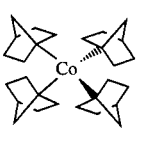
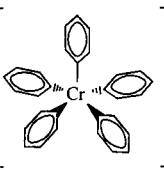
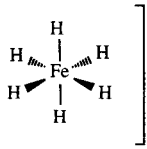
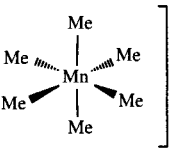
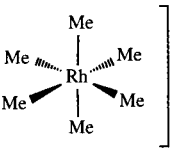
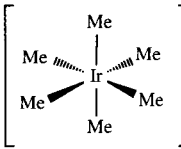
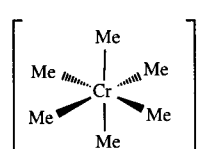
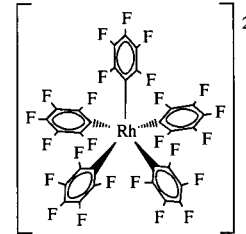
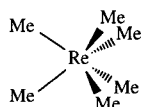
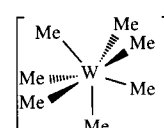
 <p>DAWFEM HV-VB XTAL a</p> <p>Mn-C 2.067 2.102</p> <p>sd<sup>0</sup> 180.0 180.0</p> <p>RMS 0.0</p>	 <p>BUJWOS HV-VB XTAL b</p> <p>Fe-C 1.987 2.058</p> <p>sd<sup>1</sup> 90.0 60.9</p> <p>90.0 60.9</p> <p>RMS 23.78 90.0 119.1</p> <p>90.0 119.1</p> <p>179.7 178.9</p> <p>179.4 178.9</p>	 <p>CIBHUQ HV-VB XTAL c</p> <p>Pt-C 2.078 2.086</p> <p>sd<sup>1</sup> 90.0 90.0</p> <p>90.0 90.0</p> <p>RMS 0.11 90.0 90.0</p> <p>90.0 90.0</p> <p>179.8 180.0</p> <p>179.8 180.0</p>	 <p>CIBJAY HV-VB XTAL c</p> <p>Pt-C 2.078 2.095</p> <p>sd<sup>1</sup> 90.0 90.3</p> <p>90.0 91.0</p> <p>RMS 1.14 90.0 88.3</p> <p>90.0 90.5</p> <p>179.8 178.8</p> <p>179.8 178.2</p>
 <p>FEBWOY HV-VB XTAL d</p> <p>Au-C 1.947 2.084</p> <p>sd<sup>1</sup> 90.0 90.0</p> <p>90.0 89.3</p> <p>RMS 0.55 90.0 90.1</p> <p>90.0 90.7</p> <p>179.8 178.9</p> <p>179.7 179.2</p>	 <p>HASZIK HV-VB XTAL e</p> <p>Ir-C 2.136 2.102</p> <p>sd<sup>1</sup> 89.1 89.2</p> <p>89.1 89.2</p> <p>RMS 4.60 91.6 90.8</p> <p>91.6 90.8</p> <p>171.3 178.4</p> <p>171.3 180.0</p>	 <p>KISDEV HV-VB XTAL f</p> <p>Mn-C 2.065 2.078</p> <p>sd<sup>1</sup> 90.0 92.4</p> <p>90.0 91.0</p> <p>RMS 9.09 90.0 91.7</p> <p>90.0 90.9</p> <p>176.9 161.8</p> <p>176.9 160.8</p>	 <p>PEXWUK HV-VB XTAL g</p> <p>Cu-C 1.995 1.966</p> <p>sd<sup>1</sup> 90.3 91.4</p> <p>90.3 89.1</p> <p>RMS 3.00 90.3 91.3</p> <p>90.3 90.2</p> <p>172.2 165.1</p> <p>172.2 172.3</p>
 <p>BUHHAN HV-VB XTAL h</p> <p>Fe-C 2.008 2.125</p> <p>sd<sup>2</sup> 90.1 102.3</p> <p>90.2 104.1</p> <p>RMS 23.83 97.1 113.9</p> <p>97.0 113.9</p> <p>101.5 113.9</p> <p>168.6 117.8</p>	 <p>YUGFOV HV-VB XTAL i</p> <p>Pt-C 2.070 2.060</p> <p>sd<sup>2</sup> 92.3 88.4</p> <p>92.3 94.8</p> <p>RMS 22.14 118.2 97.5</p> <p>118.7 99.9</p> <p>118.7 104.2</p> <p>119.2 163.1</p>	 <p>DUSPUC HV-VB XTAL j</p> <p>Co-C 1.972 1.918</p> <p>sd<sup>2</sup> 110.7 112.8</p> <p>110.0 106.5</p> <p>RMS 3.37 107.9 114.4</p> <p>109.4 108.4</p> <p>108.9 106.5</p> <p>109.9 108.4</p>	 <p>SPHENC HV-VB XTAL k</p> <p>Cr-C 2.100 2.088</p> <p>sd<sup>2</sup> 83.6 83.3</p> <p>83.6 84.3</p> <p>RMS 6.78 94.4 86.7</p> <p>94.4 95.6</p> <p>95.3 96.2</p> <p>95.3 101.2</p> <p>100.5 104.9</p> <p>100.5 109.9</p> <p>158.9 145.1</p> <p>169.3 161.3</p>
 <p>BASLIQ01 HV-VB XTAL l</p> <p>Fe-H 1.664 1.609</p> <p>sd<sup>2</sup> 90.0 89.1</p> <p>90.0 89.1</p> <p>RMS 0.74 90.0 89.2</p> <p>90.0 89.2</p> <p>90.0 89.8</p> <p>90.0 89.8</p> <p>90.0 90.2</p> <p>90.0 90.2</p> <p>90.0 90.9</p> <p>90.0 90.9</p> <p>90.0 90.9</p> <p>90.0 90.9</p> <p>180.0 178.3</p> <p>180.0 179.5</p> <p>180.0 180.0</p>	 <p>GINZEI HV-VB XTAL m</p> <p>Mn-C 2.038 2.122</p> <p>sd<sup>2</sup> 91.7 86.4</p> <p>88.2 86.4</p> <p>RMS 3.41 90.1 93.6</p> <p>90.1 93.6</p> <p>88.2 86.8</p> <p>90.1 93.2</p> <p>91.7 86.8</p> <p>90.1 93.2</p> <p>91.7 86.4</p> <p>90.1 93.6</p> <p>88.2 86.4</p> <p>177.5 180.0</p> <p>177.5 180.0</p> <p>177.5 180.0</p>	 <p>KAWVAF HV-VB XTAL n</p> <p>Rh-C 1.997 2.189</p> <p>sd<sup>2</sup> 88.7 84.8</p> <p>88.7 84.8</p> <p>RMS 8.31 88.7 84.8</p> <p>90.1 84.8</p> <p>90.1 84.8</p> <p>90.1 84.8</p> <p>90.1 87.6</p> <p>90.1 87.6</p> <p>90.1 87.6</p> <p>91.0 104.3</p> <p>91.0 104.3</p> <p>91.0 104.3</p> <p>178.4 167.6</p> <p>178.4 167.6</p> <p>178.4 167.6</p>	 <p>KAWVEJ HV-VB XTAL n</p> <p>Ir-C 1.936 2.164</p> <p>sd<sup>2</sup> 90.1 84.5</p> <p>90.1 84.5</p> <p>RMS 8.81 90.1 84.5</p> <p>90.1 84.5</p> <p>90.1 84.5</p> <p>90.1 84.5</p> <p>88.3 87.2</p> <p>88.3 87.2</p> <p>88.3 87.2</p> <p>91.6 105.6</p> <p>91.6 105.6</p> <p>91.6 105.6</p> <p>177.6 166.3</p> <p>177.6 166.3</p> <p>177.6 166.3</p>



Table 6 (Continued)

											
MCRLDX	HV-VB	XTAL o	SAHWAZ	HV-VB	XTAL p	ZOSXEL	HV-VB	XTAL q	WMe7-	HV-VB	XTAL r
Cr-C	2.093	2.300	Rh-C	2.025	2.086	Re-C	2.045	2.138			
sd <sup>2</sup>	90.0	86.2	sd <sup>2</sup>	83.0	82.2	sd <sup>4</sup>	85.8	87.0	sd <sup>5</sup>	78.9	81.3
RMS	90.0	86.2	RMS	83.0	83.3	RMS	85.8	86.8	RMS	78.9	81.3
5.73	90.0	86.2	1.71	93.4	94.7	3.26	85.8	80.4	1.23	75.0	75.6
	90.0	86.2		96.0	95.7		85.8	79.2		75.0	75.6
	90.0	86.2		96.0	96.1		85.8	80.3		146.0	146.6
	87.9	87.3		96.3	96.3		76.4	80.6		75.0	75.6
	87.9	87.3		96.3	97.2		76.4	80.0		75.0	75.6
	87.9	87.3		168.1	166.8		76.4	78.8		146.0	146.6
	92.1	101.2		173.3	169.1		133.7	134.7		75.0	75.6
	92.1	101.2					133.7	134.8		75.0	75.6
	92.1	101.2					133.7	137.3		146.0	146.6
	177.0	169.8					133.7	133.2		132.8	131.2
	177.0	169.8					133.7	133.9		132.8	131.2
	177.0	169.8					133.7	134.4		132.8	131.2
										117.7	117.2
										117.7	117.2
										117.7	117.2
										81.2	80.2
										81.2	80.2
										81.2	80.2

<sup>a</sup> Buttrus, N. H.; Eaborn, C.; Hitchcock, P. B.; Smith, J. D.; Sullivan, A. C. *J. Chem. Soc., Chem. Commun.* **1985**, 1380. <sup>b</sup> Bazhenova, T. A.; Lobkovskaya, R. M.; Shibaeva, R. P.; Shilov, A. E.; Shilova, A. K. *J. Organomet. Chem.* **1983**, 244, 265. <sup>c</sup> Uson, R.; Fornies, J.; Tomas, M.; Menjon, B.; Sunkel, K.; Bau, R. *J. Chem. Soc., Chem. Commun.* **1984**, 751. <sup>d</sup> Murray, H. H.; Fackler, J. P., Jr.; Porter, L. C.; Briggs, D. A.; Guerra, M. A.; Lagow, R. J. *Inorg. Chem.* **1987**, 26, 357. <sup>e</sup> Garcia, M. P.; Jimenez, M. V.; Oro, L. A.; Lahoz, F. J.; Tiripicchio, M. C.; Tiripicchio, A. *Organometallics* **1993**, 12, 4660. <sup>f</sup> Morris, R. J.; Girolami, G. S. *Organometallics* **1991**, 10, 792. <sup>g</sup> Naumann, D.; Roy, T.; Tebbe, K.-F.; Crump, W. *Angew. Chem. Int. Ed. Engl.* **1993**, 32, 1482. <sup>h</sup> Bazhenova, T. A.; Lobkovskaya, R. M.; Shibaeva, R. P.; Shilova, A. K.; Shilova, A. K.; Gruselle, M.; Lény, G.; Deschamps, E. *J. Organomet. Chem.* **1983**, 244, 375. <sup>i</sup> Fornies, J.; Menjon, B.; Sanz-Carrillo, R. M.; Tomas, M.; Connelly, N. G.; Crossley, J. G. *J. Am. Chem. Soc.* **1995**, 117, 4295. <sup>j</sup> Byrne, E. K.; Richeson, D. S.; Theopold, K. H. *J. Chem. Soc., Chem. Commun.* **1986**, 1491. <sup>k</sup> Muller, E.; Krause, J.; Schmiedeknecht, K. *J. Organomet. Chem.* **1972**, 44, 127. <sup>l</sup> Bau, R.; Chiang, M. Y.; Ho, D. M.; Gibbins, S. G.; Emge, T. J.; Koetzle, T. F. *Inorg. Chem.* **1984**, 23, 2823. <sup>m</sup> Morris, R. J.; Girolami, G. S. *J. Am. Chem. Soc.* **1988**, 110, 6245. <sup>n</sup> Hay-Motherwell, R. S.; Wilkinson, G.; Hussain, B.; Hursthouse, M. B. *J. Chem. Soc. Chem. Commun.* **1989**, 1436. <sup>o</sup> Krause, J.; Marx, G. *J. Organomet. Chem.* **1974**, 65, 215. <sup>p</sup> Garcia, M. P.; Oro, L. A.; Lahoz, F. J. *Angew. Chem., Int. Ed. Engl.* **1988**, 27, 1700. <sup>q</sup> Pfennig, V.; Seppelt, K. *Science* **1996**, 271, 626. <sup>r</sup> Pfennig, V.; Seppelt, K. Personal communication. <sup>s</sup> The first column lists the Cambridge Structural Database<sup>29</sup> code, the hybridization of the metal center, and the rmsd of metal-centered bond angles for HV-VB and the crystallographic structures; the second and third columns list computed and experimental metal-centered bond angles and average distances).

structure of  $[\text{Fe}(\text{naphthyl})_4]^{2-}$  is the other outlier: the HV-VB computations yield a distorted seesaw structure whereas the crystallographic structure is a slightly distorted tetrahedron. It is not clear to us what forces dominate the observed structures; Fe-C  $\pi$ -bonding, ion-pairing, and  $\pi$ -stacking among the naphthyl rings all are possible complicating features. The remaining  $sd^2$  complexes all match the experimental structures well with an average root-mean-square deviation in angles of  $5.0^\circ$ .

There are no readily available crystal structures for alkyl complexes that would be classified as hypervalent with  $sd^3$  hybridization. Examples of hypervalent molecules with  $sd^4$  and  $sd^5$  hybridization include  $\text{Re}(\text{CH}_3)_6$  and  $\text{W}(\text{CH}_3)_7^-$ , each having one 3 center-4 electron interaction. The computed structures match the experimental structures very well: the rhenium complex has a root-mean-square deviation in bond angles of  $3.26^\circ$  and  $\text{W}(\text{CH}_3)_7^-$  exhibits a root-mean-square deviation of  $1.23^\circ$ . Interestingly, our computed structure for  $\text{Re}(\text{CH}_3)_6$  has a regular trigonal prismatic ( $D_{3h}$ ) symmetry due to hypervalency rather than the  $C_{3v}$  geometries of the published structures of  $\text{Re}(\text{CH}_3)_6$  and  $\text{W}(\text{CH}_3)_6$ .

## Conclusions

This paper demonstrates that the valence concepts used for MM computations on main group compounds can be applied successfully to transition metal hydrides and alkyls. The model

gives accurate descriptions of the molecular shapes of transition metal alkyls, giving rise to an average root-mean-square deviation between calculated and observed bond angles around the metals for the 36 compounds studied of less than  $5^\circ$  per complex. At this point it is not clear that these concepts will be equally successful in describing the shapes of all transition metal complexes. For example, complexes which are highly ionic in character (such as transition metal halides or Werner complexes) or have substantial  $\pi$ -bonding (such as metal carbonyls) are objects of our ongoing research into the forces controlling the shapes of transition metal complexes.

**Acknowledgment.** We are grateful to NSF and Molecular Simulations, Inc. for partial support of this work. The generous assistance of Prof. Tony Rappè in incorporating the HV-VB terms into the UFF programs is gratefully acknowledged.

**Supporting Information Available:** A description of the force field potential energy terms and parameters used in this work is provided (7 pages, print/PDF). See any current masthead page for ordering and Web access instructions.